Tenth International Conference on Computational Fluid Dynamics (ICCFD10), Barcelona,Spain, July 9-13, 2018 **ICCFD10-265**

Three dimensional structures of flow through a square cylinder with an upstream splitter plate and for several velocity ratios.

R El Mansy*, W Sarwar **, I Rodriguez*** and JM Bergada*
Corresponding author: reda.mohamed.yousif@upc.edu

* Department of Fluid Mechanics, Turbulence and Aerodynamics Research Group (TUAREG). Universitat Politècnica de Catalunya-BarcelonaTech. Spain
** Physics Department, Universitat Politècnica de Catalunya-BarcelonaTech. Spain.
*** Turbulence and Aerodynamics Research Group (TUAREG). Universitat Politècnica de Catalunya-BarcelonaTech. Spain

1 Abstract

In the present paper, three-dimensional fluid structures and wake characteristics are evaluated for a square cylinder with an upstream splitter plate. The splitter plate divides the incoming flow in two streams, the upper and lower one, existing between them a velocity ratio. Two different Reynolds numbers of 56 and 200 and three different velocity ratios are here considered. The effect of the mixing enhancement using a square cylinder located downstream of the splitter plate is evaluated. A Floquet analysis to compute the spanwise wavelengths of three dimensional disturbances appearing in the square cylinder wake with and without a splitter plate is performed. It is observed that the use of the detached splitter plate has a stabilizing effect at low velocity ratios. However, when the velocity ratio increases, the vortex shedding suffers a linear increase and the wake resembles that of a mixing layer. Vortex dislocations appear at ratios larger than 2, which points out the onset of a bifurcation to a more chaotic wake. The wavelength of this secondary instability has been measured by means of Floquet analysis and two-point correlations being in the order of 3.5D.

2 Introduction

When studying mixing enhancement devices, the possibility of using a square cylinder located downstream of a splitter plate studied. The plate divides the incoming flow in two streams, the upper and lower one, existing between them a given velocity ratio. Given an upstream length, the separation between the cylinder and the plate, the plate length as well as the velocity ratio, are parameters studied when evaluating the device mixing performance. The attention scientific community has taken on square cylinders is much lower than what has been done on circular cylinders. Yet, there are some interesting cases where the inclusion of a square cylinder may benefit the flow performance; the ability of these devices for mixing fluids needs to be seen as one of the possible applications. Some other classical applications involve the study of towers, bridges, buildings etc.
Regarding the square cylinder configuration at low Reynolds numbers, some previous relevant works on this field were undertaken by Sohankar et al.[1, 2]. They calculated the unsteady two-dimensional flow for a square cylinder with incidence angle of ($\alpha = 0^o - 45^o$), the Reynolds number ranged from 45 to 200. They observed that with the increase of the angle of incidence, the critical Reynolds number for the onset of vortex shedding decreased. They reported that the Reynolds number at which three dimensional structures started to appear is around $150 < Re < 200$. Luo et al. [3] observed experimentally the wake

transitional modes A and B at critical Reynolds numbers 160 and 200, respectively. The spanwise length of each mode was also reported, being 5.2D and 1.2D, respectively. In a further experimental work [4], using both Laser-Induced-Fluorescent (LIF) and Particle Image Velocimetry (PIV) techniques they studied the onset of the three dimensional instabilities, confirming the similar sizes of the three dimensional structures. Later, Robichaux et al. [5], based on Floquet analysis, obtained similar results as Luo et al. [3] for modes A and B but at slightly different Reynolds numbers. They also reported a third intermediate mode called mode S, whose wavelength was in between the values reported for modes A and B. Saha et al [6] performed a three dimensional numerical study of a square cylinder for the Reynolds number range from 150 to 500, in order to analyze the critical Reynolds number for the onset of three dimensional structures. Via a time trace technique for probes placed in the near wake, and analyzing the spanwise velocity component, they observed the flow to be two-dimensional at Reynolds number of 150; three-dimensional structures were appearing at $Re = 175$. One of the recent papers published on square cylinders is the one undertaken by Mahir [7]. He performed a three-dimensional computational fluid dynamic (3D-CFD) study of the flow around a square cylinder at low Reynolds numbers 185 and 250, in order to study the heat convection around the cylinder, observing that amplitudes on the Nusselt number were particularly large on the rear face.
Regarding the use of plates around a square cylinder some of the newest papers published are [8] [9]. Both studies considered an horizontal detached flat plate located downstream of the square cylinder at low Reynolds numbers. In these papers, using two-dimensional (2D) numerical simulations, variations of lift and drag coefficients and Strouhal number were reported. In Sukri et al. [10] [11], the effect of locating an attached and detached splitter plate downstream of a square cylinder at Reynolds number 150 was numerically evaluated in 2D. Three different lengths for the attached plate were investigated; it was observed that the wake and momentum thickness kept decreasing as the splitter plate length increased. For the detached splitter plate case, the length of the plate was maintained constant and a range of distances between the plate and the cylinder were studied; two different flow regimes were observed when the plate was located at a downstream distance of 2.3D. Malekzadeh and Sohankar [12] evaluated the flow forces and the heat transfer on a square cylinder when considering a vertical detached flat plate located upstream of it. They performed a numerical 2D study at Reynolds number 160, the flat plate hight as well as the distance between the plate and the cylinder were modified. Via changing these two parameters a set of different vortex shedding configurations were reported. The Nusselt number at the front, top and bottom faces was always higher than the one observed at the rear face. Very recently, two experimental studies considering the effect of a splitter plate attached downstream of a square cylinder were undertaken. In Sarioglu [13], the plate was located downstream of a square cylinder at incidence, six different angular positions were studied, the Reynolds number was kept constant at Re=30000. Whenever the plate was considered, a sudden jump of the Strouhal number was observed. In the experimental work performed by Chauhan et al. [14] the Reynolds number was 485, three different splitter plate lengths were evaluated, vorticity, velocity contours as well as lift and drag coefficients were obtained for each case, vortex shedding was reduced as the attached plate length increased.

In the present study given an upstream length, the separation between the cylinder and the plate, the plate length and the velocity ratio, are parameters considered when evaluating the device mixing performance. For the present study, two different Reynolds numbers of $Re = 56$ and $Re = 200$ are analyzed. The Reynolds number is here defined based on the fluid velocity below the splitter plate and the cylinder lateral length. For the lowest Reynolds number, the flow is considered to be two-dimensional and for this particular case a set of velocity ratios are considered; the limit of the two dimensionality of the flow is determined by performing a Floquet analysis. At Reynolds number 200, a single distance between the plate and the square cylinder and three velocity ratios are evaluated. The effect of the splitter plate and the increasing velocity ratio in the near wake is analysed and discussed in detail.

3 Domain description

The domain to be studied is presented in figure 1. A square cylinder with side length D is placed downstream of a splitter plate. The distance between the domain inlet and the cylinder center is L_{up}=9D for all the three dimensional cases studied. Notice that the same length was used by Sohankar et al. [2], in [7] such distance was of 7.5D, in the study undertaken by [6] the upstream distance is 6.5D. For the two dimensional simulations performed, an upstream distance of L_{up}=6.5D is employed. Downstream length is fixed as L_d=25.5D. Measured from the cylinder center, upstream and downstream boundaries are located at a distance of 8D. The plate thickness is set to zero in all cases studied, as it is just used to separate the upper and lower flows. For the two dimensional cases, the plate is placed at two distances of T=2.5D and T=3.5D from the cylinder center, where as for the three dimensional cases this distance is to T=2.5D. As can be seen in figure 1, the fluid velocity above the plate is R times the base velocity below the plate.

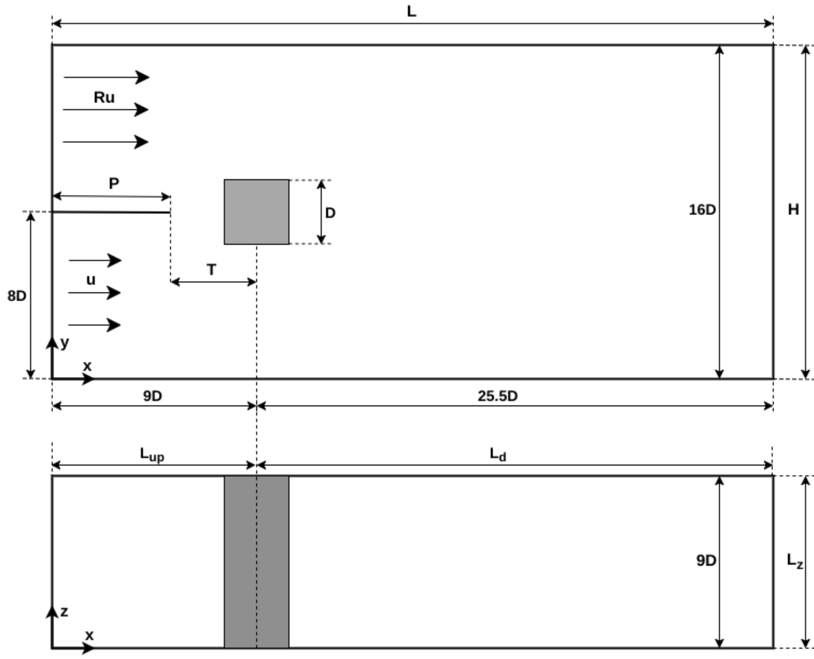

Figure 1: Computational domain used in the present study.

4 Mathematical and numerical modeling

The incompressible Navier-Stokes equations can be written as,

$$\frac{\partial u_i}{\partial x_i} = 0 \tag{1}$$

$$\frac{\partial u_i}{\partial t} + \frac{\partial u_i u_j}{\partial x_j} = -\frac{1}{\rho}\frac{\partial p}{\partial x_i} + \nu \frac{\partial^2 u_i}{\partial x_j \partial x_j} \tag{2}$$

where x_i are the spatial coordinates (or x, y, and z) in the stream-wise, cross-stream and span-wise directions. u_i (or u, v, and w) stand for the velocity components and p is the pressure. ν is the kinematic viscosity and ρ the density of the fluid. By using the cylinder diameter D and the free-stream velocity in the bottom side of the splitter plate U_∞, the Reynolds number is then defined as $Re = U_\infty\, D/\nu$.

The force per unit length acting on the body is defined by:

$$F_i = \int_S (p\delta_{ij} - \tau_{ij}) \cdot n_i dS \tag{3}$$

where δ_{ij} is the Kronecker delta, n_i is the normal vector and S is the body surface. τ_{ij} is the stress tensor and is defined as $\tau_{ij} = \mu\,(g_{ij} + g_{ji})$ with $g_{ij} = \partial u_i/\partial x_j$. The drag and lift forces are thus defined in terms of the drag and lift coefficients as,

$$
\begin{aligned}
F_d = F_1 &= \frac{1}{2} C_d \rho D U_\infty^2 \\
F_l = F_2 &= \frac{1}{2} C_l \rho D U_\infty^2
\end{aligned}
\tag{4}
$$

where C_d and C_l are the drag and lift coefficients, respectively.

For solving the problem, the following boundary conditions for both the two- and three-dimensional simulations are used. At the inlet, a constant velocity profile is imposed. On the lower side of the splitter plate, velocity profile is set to $(u, v, w) \equiv (U_\infty, 0, 0)$, where as the upper side of the plate, the inlet velocity is set to $(u, v, w) \equiv R(U_\infty, 0, 0)$, where R is the velocity ratio between the two flows. At the cylinder, no-slip boundary conditions are imposed, whereas at the outlet a pressure condition is set. As for the top and bottom boundaries, slip boundary conditions $(\partial u/\partial n, v, z) \equiv (0, 0, 0)$ are considered. For the three-dimensional cases, in the spanwise direction periodic boundary conditions are used. Considering that the problem under study has one homogeneous direction, i.e. the z-direction, the three-dimensional meshes used to solve the problem under study are obtained from the extrusion in the z-direction of a two-dimensional one. Mesh density is kept high in the vicinity of the square cylinder wall and is relaxed farther away from the cylinder in the streamwise direction.

OpenSource code Nektar++, based on spectral/hp element method framework, was used to numerically solve the incompressible Navier-Stokes-equations. This method combines the geometric flexibility of Finite element Method (FEM) and higher order accuracy of spectral methods. The computational domain consists of quadrilateral elements in the streamwise-crossflow plane with polynomial expansion of order 6. Fourier expansions have been used in the homogenous direction, i.e. z-direction. Mesh density is kept high in the vicinity of the square cylinder wall and is relaxed farther in the streamwise direction. The incompressible Navier-Stokes solver with velocity correction scheme consistent with high order pressure boundary conditions has been employed to evolve the fluid flow. The velocity and pressure fields in the velocity correction scheme are decoupled and solved independently such that the three-elliptic systems of N rank are solved instead of one-elliptic system of rank 3N. Decoupling introduces errors which can be made consistent with the overall temporal accuracy of the scheme with appropriate discretisation of pressure boundary conditions.

4.1 Grid sensitivity study

Mesh sensitivity studies for the case without the splitter plate, for Reynolds number of Re=150 are performed. This particular Reynolds number is selected in order to compare the results with those of the literature. As at this Reynolds number the flow is still two dimensional, the case is solved in a two-dimensional domain using three different meshes. The number of cells are of 84678, 95294, 121198, respectively. In order to well solve the boundary layer around the cylinder and the plate, the meshes are refined near the cylinder walls. In figure 2, a detail of the mesh refinement used is depicted. Moreover, in table 1 the minimum cell size, which corresponds with the size of the elements close to the cylinder surface is also given for all meshes. With these sizes, the maximum non-dimensional wall normal distance y^+ ($y^+ = \frac{y\, u_\tau}{\nu}$, with $u_\tau = \sqrt{(\tau_w)/\rho}$) is of 1.4, 0.3 and 0.14, respectively.

In table 1, the results obtained for the drag coefficient, the non-dimensional vortex shedding frequency $St = fD/U_\infty$ and the root-mean-square (rms) of the lift fluctuations are compared to the results from previous investigations. The error (in percentage) when compared with the finest mesh is also presented. As can be seen from table 1, the relative error of these quantities decreases as the mesh is refined. When comparing these results with those of the literature, it can be seen that results presented are also in quite good agreement. Moreover, as differences between meshes B and C are rather small and taking into consideration the computational effort required for running the three-dimensional simulations, mesh B is used as the base plane for the three-dimensional cases at Re=200.

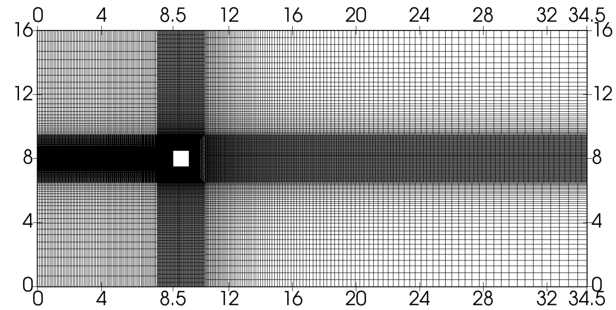

(a) Mesh 2D

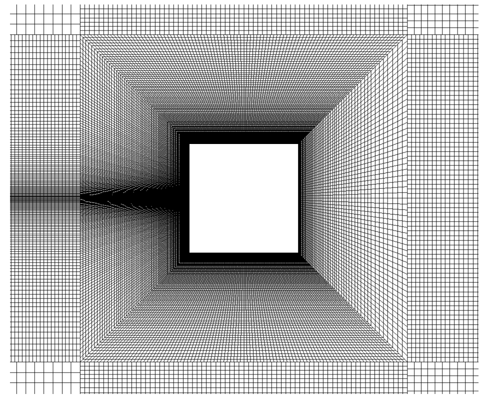

(b) Mesh 2D

Figure 2: Example of the computational mesh used in the study. (a) Overall view. (b) Detail close to the cylinder.

Table 1: Mesh refinement study at Re=150. Comparison with results from the literature. Δ_y/D, non-dimensional minimum wall normal distance, $\Delta_{min} = (\Delta_x \times \Delta_y/D^2)_{min}$, non-dimensional minimum cell size, N_{cell} total number of cells in the domain, S_t non-dimensional vortex shedding frequency, $S_t\%$ non-dimensional vortex shedding frequency relative error, C_d drag coefficient, $C_d\%$ drag coefficient relative error, C_{lrms} lift coefficient fluctuations, $C_{lrms}\%$ lift coefficient fluctuations relative error.

	Δ_y/D	Δ_{min}	N_{cell}	S_t	$S_t\%$	C_d	$C_d\%$	C_{lrms}	$C_{lrms}\%$
Mesh A	$1e^{-2}$	$1e^{-4}$	84678	0.162	+1.25	1.5426	+3.1	0.302	+5.59
Mesh B	$2.4e^{-3}$	$2.4e^{-5}$	95294	0.160	+0.0	1.50	+0.33	0.2905	+1.57
Mesh C	$1.2e^{-3}$	$1.2e^{-5}$	121198	0.160		1.495		0.286	
Wang et al.[15] Case 1		$1.7e^{-4}$		0.160		1.474		0.285	
Sukri et al.[16] Case E	$1e^{-2}$	$1e^{-4}$	228800	0.160		1.47		0.285	
Doolan.[9]				0.156		1.44		0.293	
Franke et al.[17]	$3.8e^{-3}$		6688	0.165		1.56			

4.1.1 Floquet instability analysis

The spanwise size of the computational domain can be assessed by computing the most unstable Fourier mode by instability analysis. It is reported by Luo[4] that mode B (the spanwise length for mode B should be about 1D, whereas the spanwise length for mode A is about 3-5D, see for instance [3][4][5]) should be appearing at about $Re = 204 \pm 5$, which is quite close to the Reynolds number under study. Thus, it is important to check if the spanwise length used in the present simulations is enough for containing the three-dimensional structures appearing along the spanwise direction.

In order to obtain the most unstable mode and its wavelength for $Re = 200$, and considering that the flow has a natural periodicity, a Floquet instability analysis is performed. To do this, periodic perturbations with spanwise wave number $\beta = 2\pi/\lambda_z$ are introduced to the base flow. Floquet multiplier is related to the temporal growth of the instabilities and $\mu = 1$ corresponds to zero exponential growth. In the present case at $Re = 200$ without any ratio, the most unstable mode has a wavenumber(β) of 1.207 which corresponds with a spanwise wavelength of $5.2D$, and might be related with mode A, see figure 3a. The existence of a second mode, mode B, associated to a wavenumber (β) of 5.46 and having a spanwise wavelength of $1.15D$ is to be observed in the same figure. Theses values are in good agreement with the ones reported in the literature, see [3][4][5]. Thus, in the light of the present analysis the size of the domain used in the present computations should be larger than 5.2D so as to contain the largest structures of the flow.

In order to determine the spanwise wavelength required when employing the basic Reynolds number 56 and when considering the splitter plate, a Floquet analysis is performed and presented in figure 3b. This figure introduces the Floquet analysis results from velocity ratios above 2.4, it is noticed that regardless of the velocity ratio analyzed, the maximum Floquet multiplier appears always at the same spanwise wavenumber, which means, for all these cases, the same vortex shedding mode is expected to appear. At this point it is interesting to recall that for the case of a conventional square cylinder without any splitter plate, and according to [4] mode B starts at Reynolds 204± 5. From an extension of the present Floquet analysis without the splitter plate, not presented in this paper, mode B was confirmed at Reynolds 228 as already found by [3],[4],[5],[6]. The main conclusion from the Floquet analysis presented in figure 3b, is that at Reynolds 224, corresponding to ratio 4, the first vortex shedding mode is still the same as the one appearing at lower velocity ratios. It is most likely that these effects observed to occur at low Reynolds numbers, where the flow is still 2D, are expected to be observed once the bifurcation to three-dimensional flow appears.

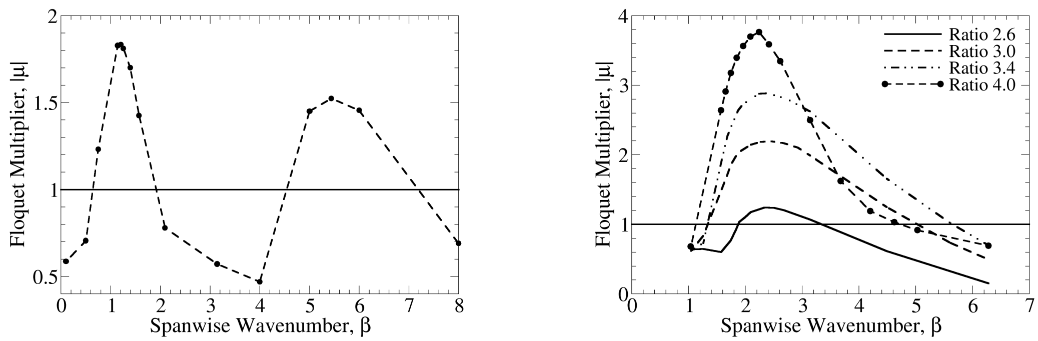

(a) (b)

Figure 3: (a) Results of the Floquet instability analysis for Re=200, no splitter plate is considered. (b) Results for the Floquet analysis study using different velocity ratios including the splitter plate in the simulation domain at basic Reynolds 56.

4.1.2 Three-dimensional mesh assessment

Owing to the previous Floquet analysis performed, the 3D structures have a spanwise wavelength of 5.2D, thus, two spanwise sizes of 9D and 18D are here considered. As commented before, three-dimensional meshes are obtained from the extrusion of a two-dimensional $x-y$ plane. Thus, for both spanwise length, a total of 32 layers are employed. Details of the meshes used are given in table 2. Notice that the mesh with a smaller spanwise size has a better resolution in the spanwise direction. In general, the final resolution obtained in the spanwise direction is comparable to the one employed by previous researchers [2][6][7], although the overall resolution in the present study is higher.

The results obtained, considering two-dimensional and three-dimensional simulations, are also presented in table 2. As can be seen, this Reynolds number is beyond the onset of three-dimensional instabilities (Re=162 as reported by [3],[4],[5]). Some differences, especially in the C_d and C_{lrms} coefficients, are observed between 2D and 3D approaches. Results obtained with the 3D mesh are in fair agreement with those reported from the literature. Notice that in terms of the global parameters, the spanwise size of the domain seems to have negligible effects, thus, simulations in the present paper are performed with the smaller domain, i.e. $L_z = 9D$ but with twice the resolution in this direction ($\Delta_z = 0.281D$ vs. $\Delta_z = 0.562D$).

Table 2: Mesh assessment at Re=200. Comparison with results from the literature. The dimensions of the domain are also given figure 1.

	S_t	C_{lrms}	C_d	L_z	L_{up}	L_d	H	N_z	Cells 2D	Cells 3D
Mesh B 2D	0.156	0.338	1.53	—	9D	25.5D	16D	0	95294	—
present 3D	0.156	0.298	1.497	18D	9D	25.5D	16D	32	95294	3.05M
present2 3D	0.154	0.285	1.493	9D	9D	25.5D	16D	32	95294	3.05M
Mahir et al.[7]	0.154	—	1.518	6D	7.5D	19.5D	15D	25	22479	0.56M
Luo et al.[4]	0.160	—	—	—	—	—	—	—	—	—
Saha et al.[6]	0.166	—	1.59	6D	6D	17.5D	10D	22	14240	0.31M
Luo at al.[3]	0.159	—	—	—	—	—	—	—	—	—
Sohankar et al[2]	0.157	—	1.39	6D	9D	12.5D	18D	25	20449	0.51M

5 Results

5.1 Flow behavior at Re=56

In this section, the Reynolds number below the plate is maintained at Re=56 and the splitter plate is located at distances of 2.5D and 3.5D from the cylinder center; a set of velocity ratios from 1 to 2.6 every 0.2 are considered. The increase in the velocity ratio leads to an asymmetric behaviour of the flow and the wake behind the cylinder. The stagnation point in the front of the cylinder moves off the center towards the top of the cylinder. As the velocity ratio increases, the maximum pressure at the stagnation point also increases (not shown in the preset paper). In figure 4, the dependence of different flow parameters with the velocity ratio is introduced. Figure 4a, presents the values of the average drag coefficient. It is interesting to see that the drag coefficient increases with the velocity ratio increase, its fluctuations also have a sharp increase as the velocity ratio increases, see figure 4b. Moreover, as the velocity ratio increases, the asymmetry of the flow increases (not shown here) which makes the lift forces to increase together with its fluctuations (see figure 4d). This induced asymmetry seems to also alter the way vortices are formed, thus increasing the vortex shedding frequency (see figure 4c). The increase of the vortex shedding frequency is linked with the increase of kinetic energy associated to the fluid, along with the decrease of the boundary layer thickness, under these conditions, the boundary layer flapping frequency increases. At this point it is interesting to recall that the vortex shedding frequency increase is particularly relevant when considering the fluid mixing enhancement. When comparing both plate distances small differences are observed at the values of $Cdrms$ and $Clrms$, 13.6% and 12.2% respectively. The frequency suffers a negligible increase as the splitter plate distance reduces. Yet, it is interesting to highlight that at ratio=1, T=2.5D, there is no vortex shedding whatsoever.

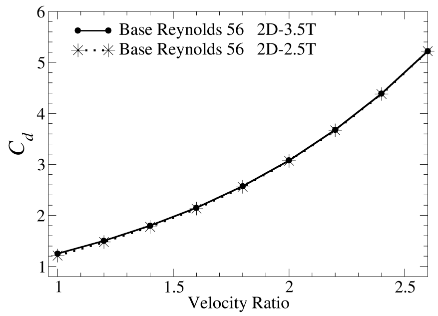

(a) Drag coefficient, C_d

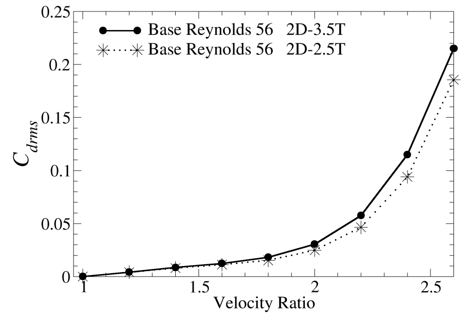

(b) Drag coefficient, C_{drms}

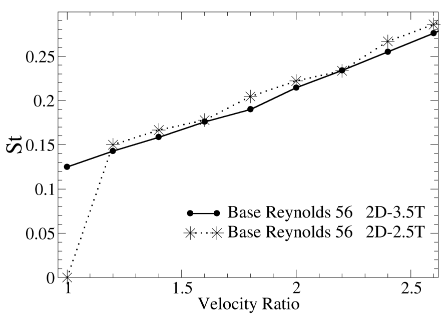

(c) Strouhal number

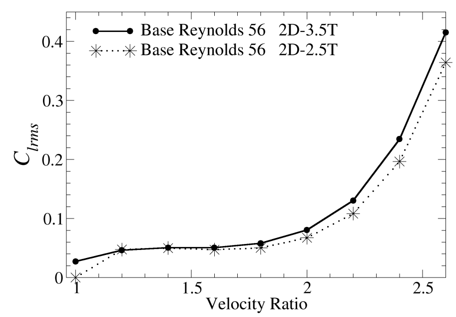

(d) Lift coefficient, C_{lrms}

Figure 4: Flow parameters as a function of the velocity ratio. (a) Drag coefficient, (b) Drag coefficient fluctuations, (c) non-dimensional vortex shedding frequency, (d) lift coefficient fluctuations. The Reynolds number below the plate is kept constant at 56.

5.2 Flow behavior at Re=200

At Re=200, the flow configuration is three-dimensional, thus important differences with the lower Re=56 are here expected. In figure 5 flow parameters are depicted. These values are also summarized in table 3. The trend for the drag coefficient, its fluctuations and the Strouhal number, appears to be the same than the one for Reynolds number 56, although, their magnitude, is smaller. On the other hand, the lift fluctuations have an opposite trend than the one at the lower Reynolds number. At Reynolds number 200, Cl_{rms} decreases as the velocity ratio increases. This decrease, as it will be shown hereafter, might probably be due to the appearance of vortex dislocations in the spanwise direction. Such vortex dislocations, which have been observed before for circular cylinders [18], are a characteristic thread of transitional flows, when the secondary instabilities appear in the wake triggering the transition from one vortex shedding mode to another.

Table 3: Three dimensional simulation results for different ratios.

Cases	St	C_d	C_{drms}	C_l	C_{lrms}
Re=200	0.154	1.493	0.012	0.0017	0.2850
Ratio 1.5	0.219	1.302	0.023	0.0550	0.0840
Ratio 2.0	0.270	2.299	0.038	0.4218	0.0815
Ratio 2.5	0.317	3.543	0.047	1.0564	0.0460

In figure 6, a segment of the time history for the drag and lift coefficients, together with the power spectrum obtained from the lift coefficient values, are presented for each studied case.

To complement this figure, the vortical structures in the cylinder wake are plotted in figure 7. Vortical structures are identified by means of Q-isocontours [19], which are contours of the second invariant of the velocity gradient tensor. This invariant identifies a vortex for Q>0, i.e. when rotation overcomes the strain.

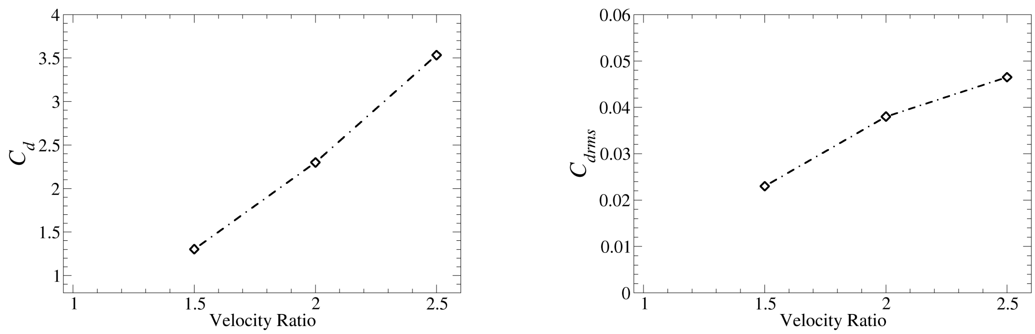

(a) Drag coefficient, C_d (b) Drag coefficient, C_{drms}

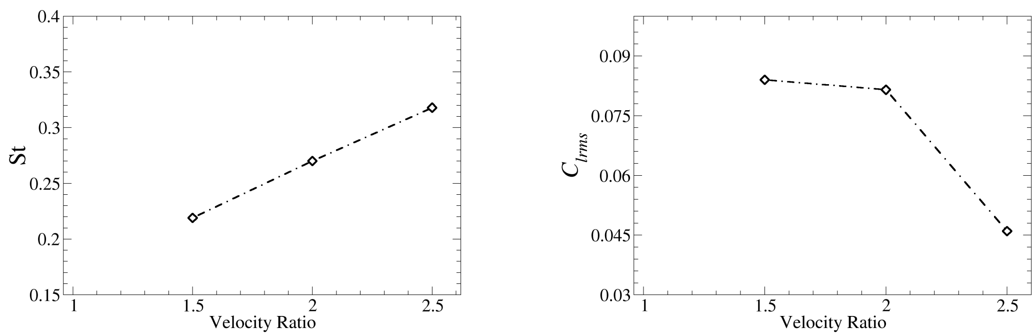

(c) Strouhal number (d) Lift coefficient, C_{lrms}

Figure 5: Drag and lift coefficients, lift fluctuations and the Strouhal number as a function of the upstream velocity ratio. The Reynolds number below the plate is kept constant at 200.

For the base case, figures 6a, b, drag and lift coefficients exhibit a low-frequency modulation typical of the square cylinder wake at these Reynolds numbers, see Sohankar et al. [2]. Figures 7 a and b, present the vortical structures for the case without plate. As expected, when there is not plate, a von Karman vortex street appears due to the shear layer flapping, thus four pairs of vortex tubes, are seen in figure 7a. The spanwise wavelength obtained via Floquet analysis is 5.2D, when performing the two-point correlation analysis using a probe line located at $(x/D, y/D) \equiv (4.5, 0.5)$ above the domain center line, a value of 5.1D is obtained. Such spanwise wavelength can be observed in figure 7a, notice as well from the same figure that the vortex tubes have a certain degree of waviness along the spanwise direction. As can be seen from figures 6d, e, at low velocity ratios the splitter plate introduces a stabilizing effect when compared with the base case. In fact, the amplitude of the lift coefficient fluctuations decreases and keep almost constant at ratio 1.5. This effect can also be observed in the vortical structures introduced in figures 7c, d. Vortical structures are much more regular than without the splitter plate, it can be stated that the splitter plate tends to make the wake more coherent. This effect is also seen at the vortex tubes as they are almost straight along the Z-direction. Based on a Floquet analysis undertaken (not included), it is determined that the spanwise wavelength is about 1.49D; the two-point correlation analysis performed on the same line probe as in the previous case, yielded a spanwise wavelength of 1.7D.

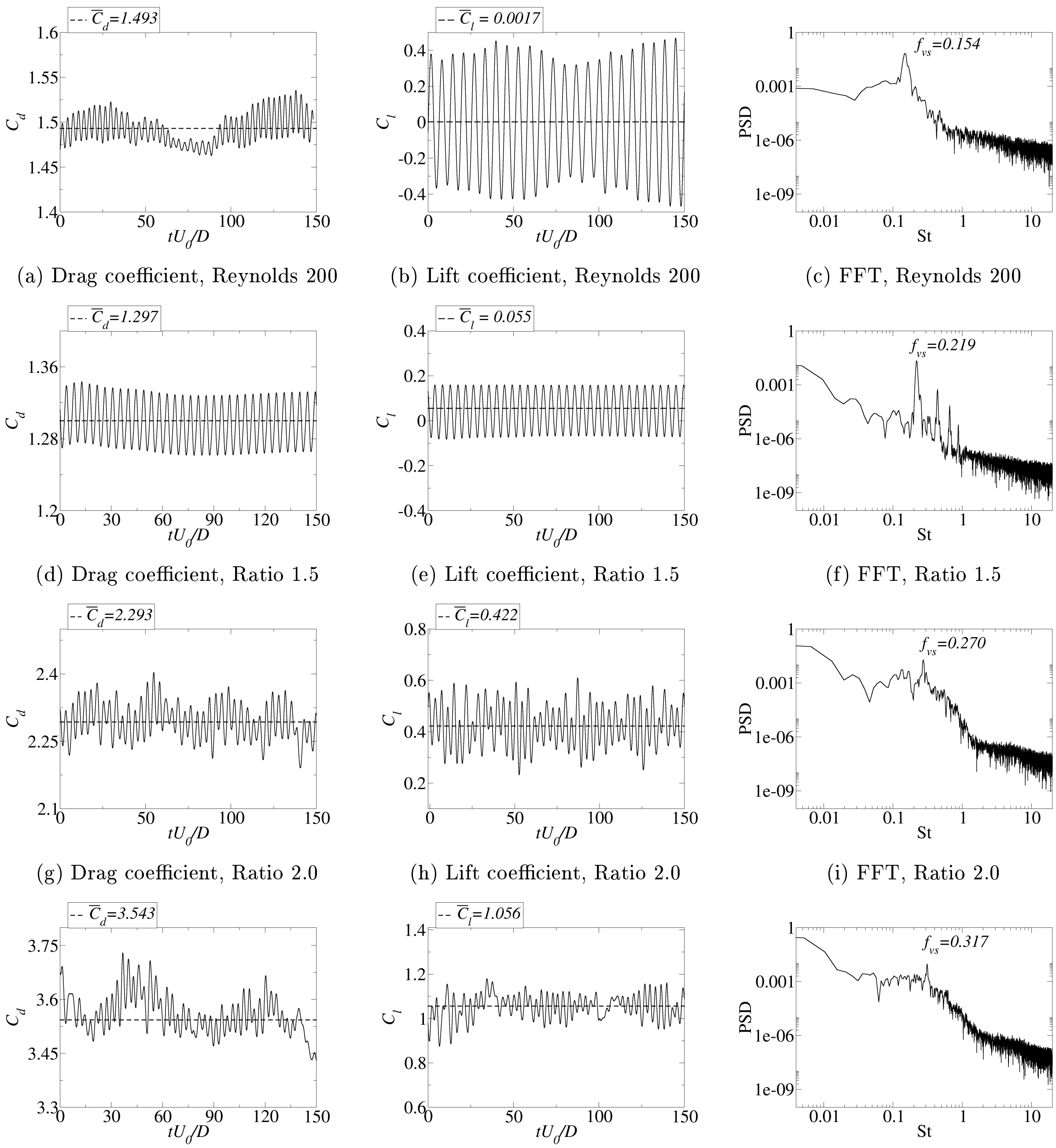

(a) Drag coefficient, Reynolds 200 (b) Lift coefficient, Reynolds 200 (c) FFT, Reynolds 200

(d) Drag coefficient, Ratio 1.5 (e) Lift coefficient, Ratio 1.5 (f) FFT, Ratio 1.5

(g) Drag coefficient, Ratio 2.0 (h) Lift coefficient, Ratio 2.0 (i) FFT, Ratio 2.0

(j) Drag coefficient, Ratio 2.5 (k) Lift coefficient, Ratio 2.5 (l) FFT , Ratio 2.5

Figure 6: Temporal evolution of the drag and lift coefficients as well as its power spectrum as a function of the velocity ratio. (a), (d), (g) and (j) drag coefficient. (b), (e), (h) and (k) lift coefficient. (c), (f), (i) and (l) power spectrum of lift fluctuations.

Both spanwise wavelength calculations clarify what is observed when comparing the figures 7a and c, the vortical structures have a much smaller spanwise wavelenght on the second case. When the splitter plate is introduced, vortices tend to be formed towards the side with the higher velocity, which in this case is above the plate. This displacement of the vortex formation changes the wake behind the cylinder which now resembles that of a mixing layer, with Kelvin-Helmholtz-like rollers in the center of the wake. Notice the well aligned vortex cores, see figures 7c and d. As these structures formed are quite regular, their footprint in the spectrum can be seen as a very energetic peak centered at $f_{vs} = 0.219$. This peak is also accompanied by three subharmonics of the main frequency, see figure 6f.

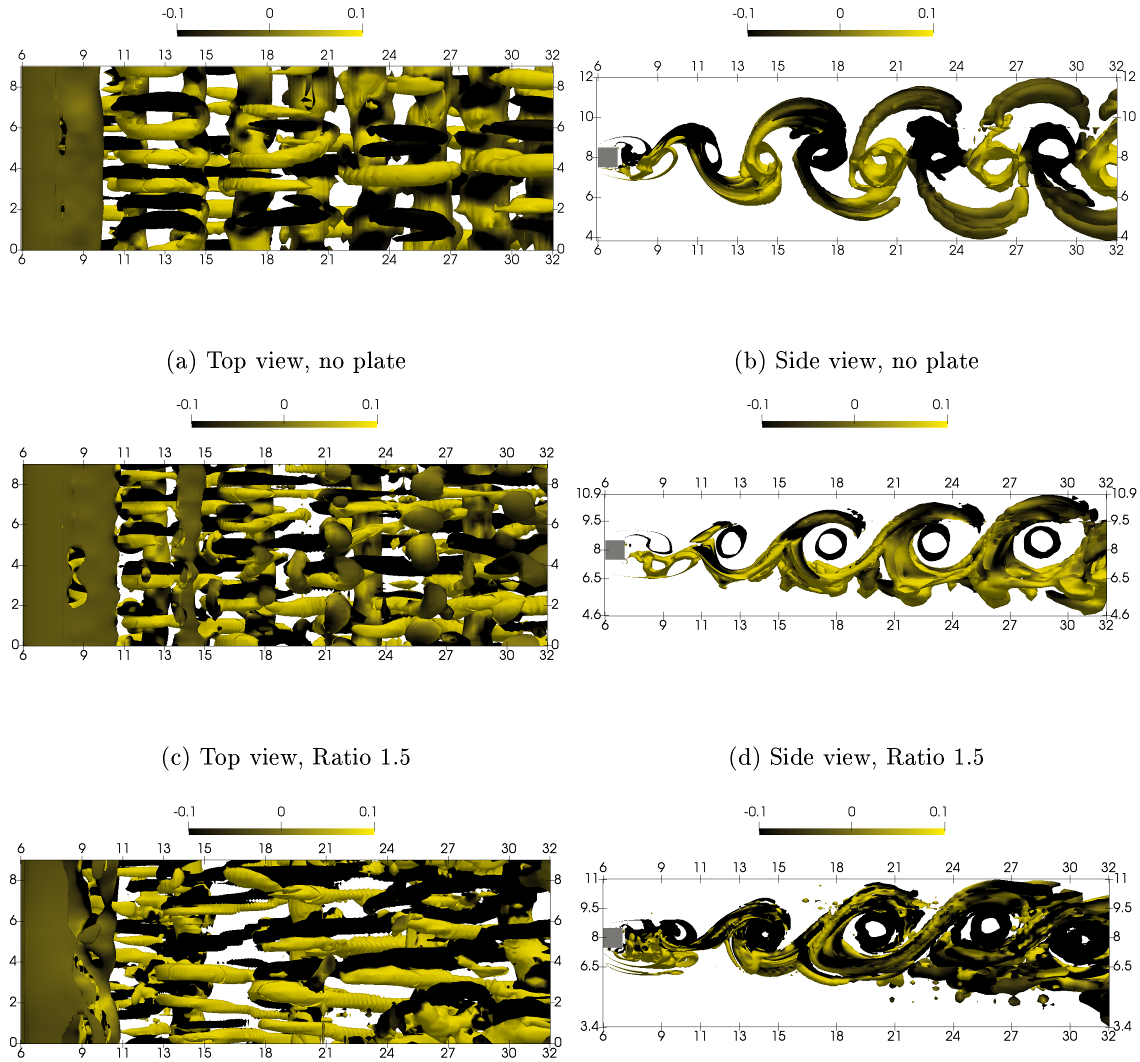

(a) Top view, no plate

(b) Side view, no plate

(c) Top view, Ratio 1.5

(d) Side view, Ratio 1.5

(e) Top view, Ratio 2.5

(f) Side view, Ratio 2.5

Figure 7: Vortical structures at different velocity ratios represented by means of Q iso-contours.

At velocity ratios larger than 1.5, Kelvin-Helmholtz instabilities are the ones driving the downstream vorticity. The vortex generated from the square cylinder upper side is more energetic than the one generated below the cylinder. The low energetic vortex, once reaches the cylinder trailing edge, collapses and the upper cylinder vortex takes control of the downstream vortex formation. The same phenomenon of vortex formation is taking place at different velocity ratios see, figures 7e, f and c, d. As the velocity ratio increases from 1.5 to 2.5, a new transition takes place in the vortex formation zone and vortex dislocations start to occur. Around ratio 2.5, a secondary instability with spanwise wavelength of about 3.48D- 3.52D appear, (based on Floquet and two-point correlations analysis, respectively). It seems thus, that around ratio 2.5 the wake is at the onset of a bifurcation to a more chaotic state, as can also be seen from the more irregular pattern of the vortex cores and ribs connecting them (see figure 7 (e-f)). Actually, the more chaotic nature of the vortex shedding can readily be seen from the time history of the drag and lift coefficients (see also figure 6 (j-k)), where, as aforementioned, lift fluctuation amplitude decreases. This loss of coherence due to the transition into a more chaotic state produces a smaller peak in vortex shedding frequency (see figure 6 (i-l)) if compared to that observed at ratio 1.5.

6 Conclusions

The effects of locating a splitter plate with different velocity ratios in front of a square cylinder are studied at Reynolds number 56 and at Reynolds number 200.At both Reynolds numbers, the increase in the velocity ratio produce an increase in both drag coefficient and vortex shedding frequency.

For the larger Reynolds number, i.e. Re=200, different changes in the wake are observed. At lower velocity ratios, the splitter plate introduces a stabilizing effect while at the same time the wake changes from the von Karman vortex street typical of bluff bodies wakes to one driven by Kelvin-Helmholtz rollers associated to mixing layers. The stabilizing effect of the plate at ratio 1.5 produces a more coherent vortex shedding with a energetic peak centered at 0.219.

As the velocity ratio increases, the wake losses its coherence and vortex dislocations are observed with a spanwise length of 2.5D which seems to point out the onset to a more chaotic state.

7 Acknowledgements

We are very thankful to the Red Espanola de Supercomputacion (RES) network of supercomputers for providing the necessary computing resources for this project. Also, this work is conducted as part of the Spanish government funded research grant, FIS2016-77849-R, in the duration of 2017-2020.

References

[1] A Sohankar, C Norberg, and L Davidson. Low-Reynolds-number flow around a square cylinder at incidence: study of blockage, onset of vortex shedding and outlet boundary condition. *International Journal for Numerical Methods in Fluids*, 26(1):39–56, 1998.

[2] Ahmad Sohankar, C Norberg, and L Davidson. Simulation of three-dimensional flow around a square cylinder at moderate Reynolds numbers. *Physics of Fluids*, 11(2):288–306, 1999.

[3] SC Luo, YT Chew, and YT Ng. Characteristics of square cylinder wake transition flows. *Physics of Fluids*, 15(9):2549–2559, 2003.

[4] SC Luo, XH Tong, and BC Khoo. Transition phenomena in the wake of a square cylinder. *Journal of Fluids and Structures*, 23(2):227–248, 2007.

[5] J Robichaux, S Balachandar, and SP Vanka. Three-dimensional floquet instability of the wake of square cylinder. *Physics of Fluids*, 11(3):560–578, 1999.

[6] AK Saha, G Biswas, and K Muralidhar. Three-dimensional study of flow past a square cylinder at low Reynolds numbers. *International Journal of Heat and Fluid Flow*, 24(1):54–66, 2003.

[7] Necati Mahir. Three dimensional heat transfer from a square cylinder at low Reynolds numbers. *International Journal of Thermal Sciences*, 119:37–50, 2017.

[8] Shams Ul Islam, Hamid Rahman, Waqas Sarwar Abbasi, Uzma Noreen, and Aftab Khan. Suppression of fluid force on flow past a square cylinder with a detached flat plate at low Reynolds number for various spacing ratios. *Journal of Mechanical Science and Technology*, 28(12):4969–4978, 2014.

[9] Con J Doolan. Flat-plate interaction with the near wake of a square cylinder. *AIAA journal*, 47(2):475–479, 2009.

[10] Mohamed Sukri Mat Ali, Con J Doolan, and Vincent Wheatley. Low Reynolds number flow over a square cylinder with a splitter plate. *Physics of Fluids*, 23(3):033602, 2011.

[11] Mohamed Sukri Mat Ali, Con J Doolan, and Vincent Wheatley. Low Reynolds number flow over a square cylinder with a detached flat plate. *International Journal of Heat and Fluid Flow*, 36:133–141, 2012.

[12] S Malekzadeh and A Sohankar. Reduction of fluid forces and heat transfer on a square cylinder in a laminar flow regime using a control plate. *International Journal of Heat and Fluid Flow*, 34:15–27, 2012.

[13] Mustafa Sarioglu. Control of flow around a square cylinder at incidence by using a splitter plate. *Flow Measurement and Instrumentation*, 53:221–229, 2017.

[14] Manish Kumar Chauhan, Sushanta Dutta, Bhupendra Singh More, and Bhupendra Kumar Gandhi. Experimental investigation of flow over a square cylinder with an attached splitter plate at intermediate Reynolds number. *Journal of Fluids and Structures*, 76:319–335, 2018.

[15] Jiansheng Wang, Yakun Xu, and Haojie Cheng. Features of flow past square cylinder with a perforated plate. *Transactions of Tianjin University*, 22(6):544–554, 2016.

[16] Mohamed Sukri Mat Ali, Con J Doolan, and Vincent Wheatley. Grid convergence study for a two-dimensional simulation of flow around a square cylinder at a low Reynolds number. In *Seventh International Conference on CFD in The Minerals and Process Industries (ed. PJ Witt & MP Schwarz)*, pages 1–6, 2009.

[17] R Franke, W Rodi, and B Schönung. Numerical calculation of laminar vortex-shedding flow past cylinders. *Journal of Wind Engineering and Industrial Aerodynamics*, 35:237–257, 1990.

[18] CHK Williamson. The natural and forced formation of spot-like vortex dislocations in the transition of a wake. *Journal of Fluid Mechanics*, 243:393–441, 1992.

[19] JCR Hunt. Stream and convergence zones in turbulent flows. *Center for Turbulence Research Report*, 1988.